Waalbot: An Agile Small-Scale Wall Climbing Robot Utilizing Pressure Sensitive Adhesives

Michael P. Murphy, William Tso, Michael Tanzini, Metin Sitti
Department of Mechanical Engineering, Carnegie Mellon University, Pittsburgh, Pennsylvania 15213

***Abstract*— This paper proposes a small-scale agile wall climbing robot able to navigate on smooth surfaces of any orientation, including vertical and inverted surfaces, which uses adhesive elastomer materials for attachment. Using two actuated legs with rotary motion and two passive revolute joints at each foot the robot can climb and steer in any orientation. Due to its compact design, a high degree of miniaturization is possible. It has onboard power, sensing, computing, and wireless communication which allow for semi-autonomous operation. Various aspects of a functioning prototype design and performance are discussed in detail, including leg and feet design and gait control. The current prototype can climb 90° slopes at a speed of 6 cm/s and steer to any angle. This robot is intended for inspection and surveillance applications and, ultimately, space missions.**

I. Introduction

Mobile robots with the ability to climb and navigate on surfaces of any orientation without leaving residue or damaging the surface have many potential applications. One of the most notable situations where such a robot could be useful, and perhaps life-saving, is for spacecraft hull inspection and repair. Terrestrial uses include surveillance or inspection in hazardous or difficult to reach areas.

Researchers have proposed a great variety of climbing robots for various applications. Many of the first wall scaling robots were intended for cleaning in hazardous environments such as nuclear reactors [1]. In general, climbing robots use one of three types of attachment mechanisms; vacuum suction [1]–[7], magnetic attraction [8], or gripping with claws or grasping mechanism [9], [10]. Each of these mechanisms has advantages and drawbacks. For instance, magnetic attraction can be very strong and can have good power failure mitigation, but is only applicable for ferromagnetic surfaces. Suction adhesion relies on a good seal with the surface, so cracked or non-smooth surfaces are problematic and power efficiency limits their untethered climbing duration. Recently, robots using micro-claws have shown good performance on surfaces such as brick and stone [9], but clawed and grasping robots cannot climb smooth surfaces like glass or painted structures. To avoid the drawbacks associated with the aforementioned climbing mechanisms, the robot presented in this paper is designed to ultimately utilize a different type of adhesion mechanism found in biology called dry adhesion.

This paper proposes a semi-autonomous small-scale robot theoretically capable of navigating on smooth flat surfaces of any orientation using adhesive elastomer for attachment. The robot is actuated by two motors, each controlling a set of three-footed wheels. Unlike many previous implementations

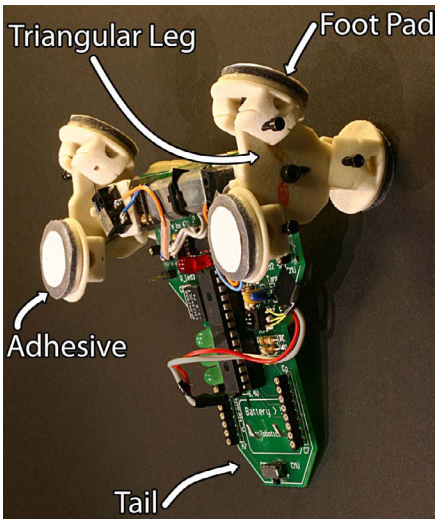

Fig. 1. Photograph of prototype Tri-Foot Waalbot climbing a 90° (vertical) surface.

of wheel-leg designs such as the ground walking RHex [11], Whegs [12] and miniWhegs [13] robots, Waalbot's legs are specialized for climbing. A Mini-Whegs climbing robot has been developed which is able to climb and transition reliably using adhesive tape, but can only steer very gradually [14]. In contrast, Waalbot climbs with high speed and is able to make sharp turns.

II. Attachment Mechanism

The Gecko lizard's ability to climb surfaces, whether wet or dry, smooth or rough, has attracted scientists' attention for centuries. By means of compliant micro/nano-scale high aspect ratio beta-keratin structures at their feet, geckos and spiders manage to adhere to almost any surface with a controlled contact area [15]. It has been shown that adhesion is mainly due to molecular forces such as van der Waals forces [16] (from which Waalbot draws its name). Tiny fibers on the animals feet form weak attractive bonds with the surface, the combination of billions of contacting fibers creates a large adhesion (up to 100 kPa). Since dry adhesion does not rely heavily on the surface material or atmospheric pressure, it allows climbing on a wide variety of surfaces and is uniquely suitable for use in the vacuum of space.

Synthetic fibrillar dry adhesive technology is not currently mature enough to be used for climbing robots, however Waalbot is designed with the intention of eventually utilizing the

technology. While efforts to develop the synthetic fibrillar dry adhesive continue, the robot uses polymer adhesive material (Smooth-On Vytaflex 10) which shares many performance characteristics with the envisioned dry adhesive material. Both the dry adhesive and the elastomer adhesive must be pressed to the surface with a preload force in order to provide an adhesive force on detachment. Like fiber based biological adhesives, elastomers gain their adhesion performance by deforming into the microscale surface features of any smooth surface and creating a large contact area. Using these adhesives as substitutes until the fiber based dry adhesives have suitable performance for this application allows testing and improvements to the robot design.

The adhesive elastomer is characterized for its adhesion through testing on a custom system. A sample is moved into contact with a substrate which is connected to a high resolution load cell by an automated stage. When the pressing force reaches a given preloading value the sample is retracted. The adhesive force is recorded as the maximum force before separation and the force values are converted to pressures by dividing by the area of the sample. Figure 2a is a force versus time chart showing the preload (point **A**) and maximum adhesion value (point **B**) for a single experiment. A series of these experiments is performed by varying the preload value and a plot of the adhesion results forms a performance curve (Fig. 2 b) for the adhesive-substrate combination. This performance curve shows typical behavior for an adhesive elastomer. The adhesion is greater than the preload pressure for low preload pressures. For higher preload pressures the performance curve levels off at a maximum adhesion value.

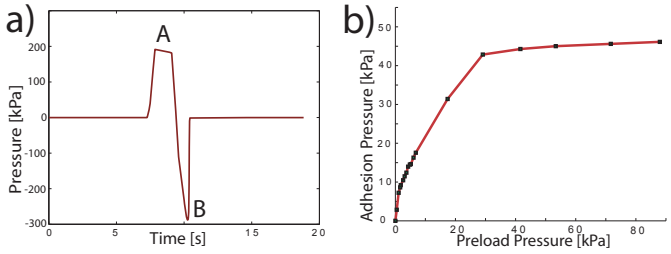

Fig. 2. Force vs. time data plot for a single adhesion test (**a**) and performance curve for V10 on Acrylic (**b**).

III. Robot Design

A. Mechanical Design

In order to create the preload force sufficient to bring the adhesive into intimate contact with the surface, the robot should be designed to maximize the pressing force when the adhesive pads come into contact with the climbing surface. This requirement guides the design of the legs and feet mechanisms. A gear motor's output shaft is connected to a triangular shaped leg, where each point of the triangle holds a foot assembly on a revolute ankle joint (Fig. 3). The ankle joint assembly is spring loaded to always return to the forward position (the robot cannot travel in reverse).

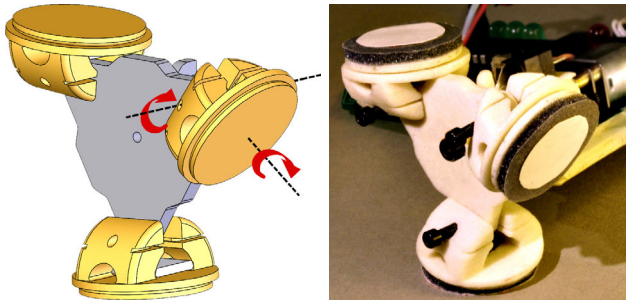

Fig. 3. CAD model of the Tri-Foot design (left) and assembled prototype components (right). Each foot pad has two degrees of freedom enabling climbing and steering.

On the distal end of the foot assembly is a passive revolute joint connecting a foot pad which holds the adhesive material. This distal joint enables steering capabilities (discussed later in Section IV).

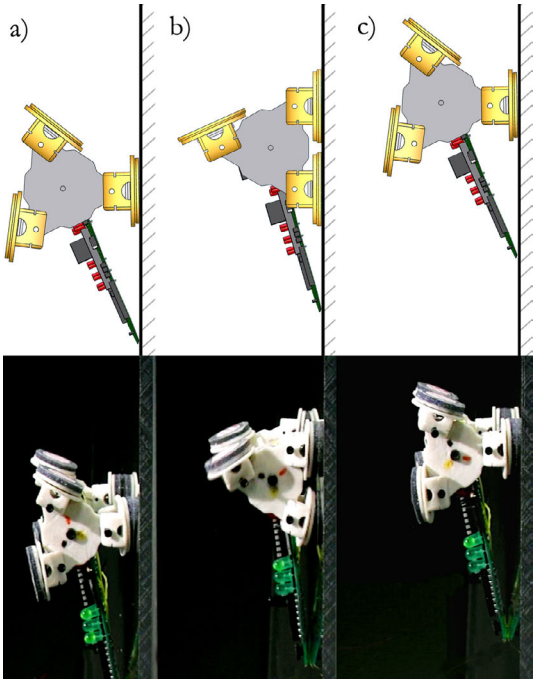

Fig. 4. Schematic side view of Waalbot climbing a vertical surface (top) and still photo frames from a video of the Waalbot prototype performing the same actions (bottom).

The principle of operation is as follows. During forward travel the two legs are synchronized and step in unison. As the motors turn, the tail of the robot presses against the surface and the triangular legs rotate forward. The two feet which are adhered to the surface (one on each side) support the weight of the robot (Fig. 4a). Soon the forward feet come into contact with the surface (Fig. 4b). At this time there are 5 contact points with the surface; 2 feet on each side and the tail. The motor torque provides an internal moment which presses the front feet onto the surface while pulling the rear feet away from the surface. When the rear foot normal force F_{Rn} reaches a critical peeling value of F_{cr}, the adhesive peels away from the surface and the robot steps forward (Fig. 4c).

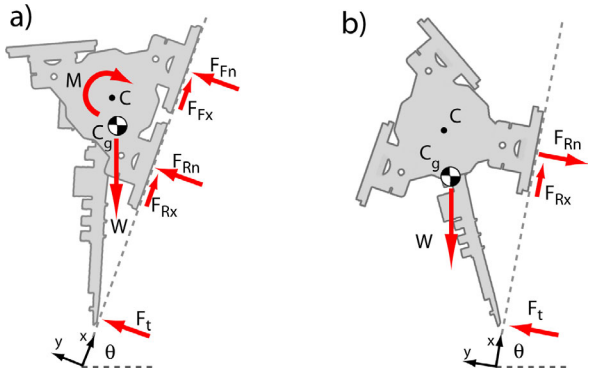

Fig. 5. Free body diagrams showing the forces during a forward step where the front foot is pressed against the surface and the rear foot is peeled (left), and in the configuration in which the robot experiences the highest peeling force while climbing (right).

Examining the free body diagram (Fig. 5a) and assuming quasi-static dynamics and symmetric loading it is possible to find a system of equations which describe the forces on the robot during the stepping transfer:

$$\begin{aligned}\sum F_y &= 0 = F_t + F_{Rn} + F_{Fn} - W\cos\theta \\ \sum F_x &= 0 = F_{Rx} + F_{Fx} - W\sin\theta \\ \sum M_c &= 0 = M + (F_{Rn} - F_{Fn})(\frac{d_{step}}{2}) \\ &\quad + F_t(L_t) + W\sin\theta(L_{yc} - L_{ycg}) \\ &\quad -(F_{Rx} + F_{Fx})(L_{yc}) - W\cos\theta(L_{xcg})\end{aligned} \tag{1}$$

where M is the motor torque, W is the weight, θ is the slope of the climbing surface, F_t, F_{Rn}, F_{Fn} are the normal forces at the tail, rear foot, and front foot respectively. F_{Rx} and F_{Fx} are the shear forces on the rear and front feet respectively. d_{step} is the distance between the centers of the rear and front feet, L_{yc} is the distance from the climbing surface to the center of the leg, and L_{ycg}, L_{xcg} are the distances from the center of gravity (C_g) to the surface and center of the leg respectively. L_t is the distance between the center of the leg and the tail-surface contact point.

There are five unknown forces ($F_{Fn}, F_{Rn}, F_{Fx}, F_{Rx}, F_t$) and only three equations, so in order to solve for the unknowns some assumptions must be made. Assuming $F_{Rn} = F_{cr}$ will give the forces just before the peel-off occurs, which is when F_{Fn} is at a maximum. We also assume that the shear forces on the front and rear feet are equal ($F_{Fx} = F_{Rx}$). Lastly we assume that the torque just before peel-off is equal to the torque necessary to peel the rear feet and preload the front feet with an equal force ($M = 2{\cdot}F_{cr}{\cdot}d_{step}/2 = F_{cr}{\cdot}d_{step}$). This assumption also guides the minimum motor torque requirements when designing the prototype robot.

Using these assumptions and (1) it is possible to examine the effect of slope angle θ on the preload force F_{Fn}. Since this preload force is essential for creating intimate contact and thus adhesion, it is of critical importance. Specifically, the ratio between the critical peel-off force F_{cr} and the preload force determines the requirements for the adhesive. Using the Waalbot prototype geometry and specifications the relationship between this ratio and the slope angle is found (Fig. 6).

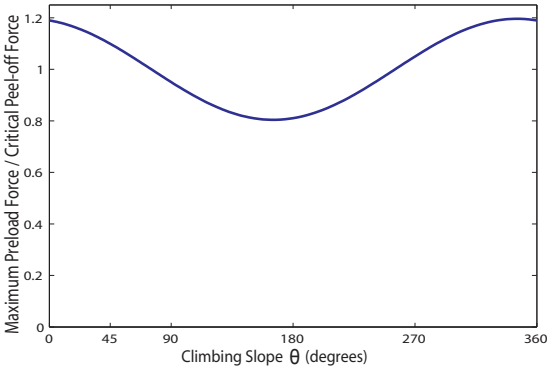

Fig. 6. Plot of preload/peeling force ratio for various values of slope angle θ generated from (1).

The graph indicates that for the prototype Waalbot there is a change of this ratio of up to 33% depending on the climbing angle, with a maximum preload force at $345°$ (climbing slightly downhill) and a minimum at $165°$ (close to inverted climbing). The lowest ratio has a value of 0.80, meaning that for sustainable climbing, the adhesive must provide 1.25 times as much adhesion as the force it was preloaded with, otherwise the robot will lower the F_{cr} with each step. As we will show below, if this value drops below a certain value, the robot will fall from the wall during climbing.

The adhesives used with the robot have high shear adhesion and therefore detach from the normal forces pulling the foot away from the surface. The minimum adhesion normal force required to keep the robot attached to the wall during climbing can be found by examining the case when only one foot per side is attached and the C_g is at its furthest distance from the surface. The quasi-static equation for this configuration (Fig. 5b) gives a maximum force which the adhesives must be able to provide:

$$F_{Rn} = \frac{W}{L_t}\left(L_{ycg(max)}\sin\theta - (L_t - L_{xcg})\cos\theta\right) \tag{2}$$

If this force exceeds the magnitude of F_{cr} then the robot will detach from the surface. Therefore, this equation gives the minimum adhesive performance needed to climb. Of course, because of the consequences of a fall, a safety factor is used when choosing an adhesive and adhesive foot area. Graphing this function with the known design parameters of the robot it is possible to find the maximum peeling force over all angles (Fig. 7). For the prototype parameters the maximum peeling force occurs at a climbing angle of $165°$. From this graph it is seen that the critical peeling force of the adhesive F_{cr} must be greater than 0.7 N for climbing on surfaces of all possible orientations.

From (2) it is clear that in order to minimize the peeling force on the adhesive pad during climbing, the length of the tail should be increased and also the center of gravity should be moved close to the wall. Finally the weight of the robot should be minimized. This may be accomplished through fabricating

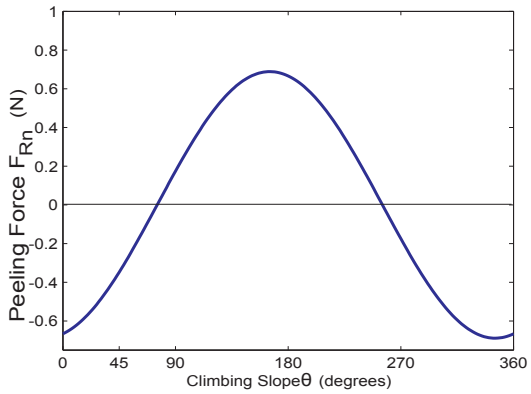

Fig. 7. Plot of the minimum normal peeling force which the adhesives must overcome for the robot to climb a slope of angle θ.

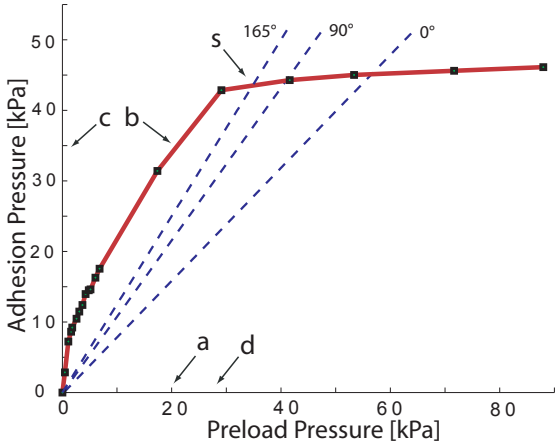

Fig. 8. Performance plot showing converging behavior to the steady state operating point (**s**).

the robot from lighter materials or through miniaturization. Miniaturization is advantageous to this robot design because mass is proportional to L^3 while the adhesion is proportional to area, thus L^2. As the robot shrinks in size, the adhesion will be reduced less than the gravitational force, so we will see an increase in the climbing abilities of the robot.

Both (1) and (2) suggest that the tail should be long to increase preload force and to minimize the peeling force. However, it is important to note that the weight of the robot is also increased with the tail length, so there is a coupling between W and L_t which is also discussed in previous work [17]. Furthermore, a longer tail increases the amount of room necessary for turning, as the tail may sweep out and contact obstacles causing the robot detach from the surface and fall, so a longer tail limits the ability to climb in small areas. Therefore, for maximum performance without compromising agility the tail length is chosen to be the longest length such that the tail remains fully within the turning circle (Fig. 10).

B. Adhesive Requirements

The values from Figs. 6 and 7 create a set of requirements for the adhesive used. For the Waalbot to have the ability to climb on surfaces of all slopes, the operating critical peeling force must be no less than 0.7 N (from Fig. 7) and the adhesive must hold with a minimum of 1.25 times as much force as it was preloaded with (from Fig. 6) at this operating peeling force. To visualize such a requirement it is convenient to plot an adhesive-substrate performance curve with bounds which represent the requirements as in Fig. 8. Using this representation it is possible to determine if an adhesive is suitable, and if it is, what the minimum contact area must be.

In Fig. 8 the performance curve is plotted along with a line with a slope of 1.25 called the 'ratio line' for $\theta = 165°$. The slope is the inverse of the ratio of adhesion to preload (from Fig. 6) for the case when the robot is climbing on a surface oriented at $165°$ which was found to be the most challenging (from Figs. 6, 7). Each surface orientation slope has an associated ratio line. Ratio lines for surface orientations of $90°$ (wall) and $0°$ (floor) are also plotted in Fig. 8 for reference. The slopes of these lines are found directly from the inverses of the values for corresponding surface angles in Fig. 6.

If the robot starts with an arbitrary initial preload of 20 kPa (Fig. 8 point **a**) following the chart up to the performance curve (point **b**) we see that the resulting adhesion is approximately 35 kPa (point **c**). This maximum adhesion pressure (peeling pressure) is transferred to the preload pressure for the next step through (1). Considering the case when the robot is climbing on a surface of $\theta = 165°$ the ratio of adhesion to preload is 0.8 (from Fig. 6), so the preload for the next step is $35 * 0.8 = 28$ kPa (point **d**). Repeating this procedure, the preload and adhesion values will converge to the intersection point of the 'ratio line' and the performance curve (point **s**) in a few steps. The values will also converge to this point if the initial preload value is to the right of point **d**, as can be seen by repeating this exercise with a high initial preload.

Point (**s**) in Fig. 9, the steady state operating point, has an associated steady state operating adhesion pressure (**e**) and preload pressure (**h**). There is also a minimum safe adhesion value (**f**) which is a function of the area of the footpads and the surface slope angle θ and can be calculated from (2) and foot size. Figure 9 also shows the associated minimum safe preload (**g**). The steady state operating adhesion (**e**) must be greater than the minimum safe adhesion value (**f**) to prevent the robot from detaching from the climbing surface. The margin between the steady state operating adhesion (**e**) and the minimum safe adhesion (**f**) is the margin of safety. Since the robot will not always have ideal force transfer on every step, it is important to have a large margin of safety so that the robot can recover from a problematic step, or continue to operate if the adhesives become contaminated and function with degraded performance.

It is possible to increase the margin of safety by increasing the area of the adhesives (foot pad size) which lowers the minimum adhesion pressure requirement, however, there is a trade-off because the motor then needs to provide more torque to peel the larger feet. This causes an increased power require-

ment, which leads to bigger batteries, and also necessitates larger heavier motors.

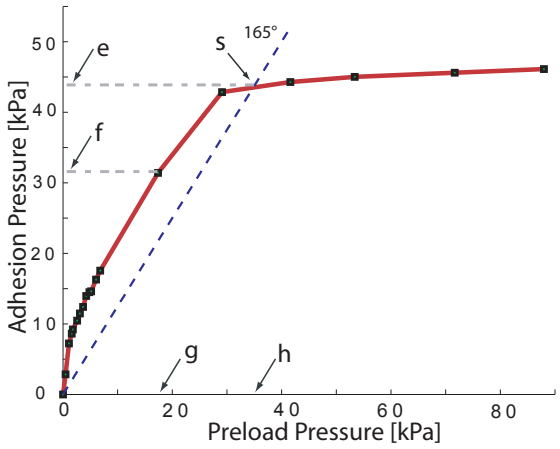

Fig. 9. Performance plot showing the minimum adhesion requirement (**f**), minumum safe preload (**g**), and steady state operating points (**s**, **e**, and **h**) for climbing a surface of $\theta = 165°$.

C. Robot Fabrication

A printed circuit board (PCB) acts as the chassis for the robot. The leg and feet assemblies are fabricated via 3D printing (Z-corp). The heaviest components of the system are the leg assemblies, motors, and batteries. In order to move the center of gravity as close as possible to the surface and balanced around the motor axes, all of these parts are located close to the motors, with the batteries beneath the PCB, nearly in contact with the climbing surface.

The robot is controlled by a PIC microcontroller (PIC16F737) and is able to perform pre-programmed actions such as climbing and turning. Gait is controlled with feedback from foot position sensors. Limit switches are triggered when the legs are aligned such that only one foot on each side is contacting the surface. This information is used to keep the robot's gait synchronized by pausing one of the motors until the opposing motor catches up, so that the assumptions of symmetry in (1) are valid. The sensors are also important for safely putting the robot into steering mode.

Infrared (IR) RC5 communication is used to command the robot to climb straight, stop, or turn. Commands can be sent for turning $180°$, $90°$, and in increments of $15°$ in either direction.

Power is provided by two lithium ion polymer batteries beneath the robot body. The two motors (Sanyo 12GA-N4s) have a torque output of approximately 400 mN·m each, which is sufficient to peel the rear feet from the surface.

IV. Agility

A. Steering

When only one foot on a side is contacting the surface, that foot can be used as a pivot point for the robot to turn around. By advancing the opposite motor, the robot rotates around the passive revolute joint in the pivoting foot. If the robot attempted to turn while two feet were attached on a side, the robot would shear itself off of the surface since the center of rotation would not be aligned with a joint. This can be a catastrophic failure for a climbing robot, so the foot position sensors are used to prevent this occurrence.

In steering mode, the robot takes discrete steps around the pivoting foot. The turning radius is less than the width of the robot so tight turns are possible (Fig. 10). The ability to make tight turns is an important feature for climbing through small passageways or for avoiding closely spaced obstacles.

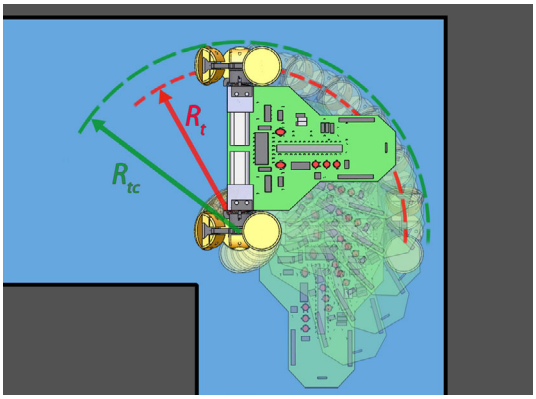

Fig. 10. Waalbot's small turning radius (R_t) and turning circle radius (R_{tc}) let it climb around obstacles and operate in narrow corridors with sharp bends (top).

Steering angle per step can be calculated from the turning radius R_t and the stepping distance d_{step} as follows:

$$\theta = \cos^{-1}\left(1 - \frac{d_{step}^2}{2R_t^2}\right) \tag{3}$$

where the turning radius R_t is the lateral distance between the centers of the feet. Conversely, given a desired stepping angle, the robot's dimensions can be designed to achieve this angle.

The prototype Waalbot was designed to make discrete turning increments which change the heading by $15°$ per step. This angle is convenient as it allows for turns of $45°, 90°, 180°$ as well as smaller adjustments.

V. Experiments

A prototype Waalbot was built according to the design aspects previously mentioned with the specifications given in Table I.

Mass	100 g
Length	13 cm
Height	5 cm
Width (total)	12.3 cm
Turning Radius (R_t)	10 cm
Turning Circle Radius (R_{tc})	11.15 cm
Step Length (d_{step})	2.6 cm
Adhesive Area (per foot)	1.1 cm^2
Speed	6 cm/s
Turning Speed	37.5°/s

TABLE I

Specifications of the robot prototype in experiments

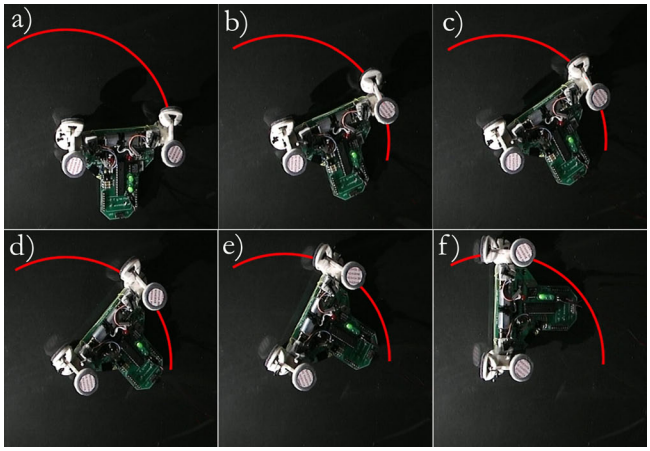

Fig. 11. Still frames from a video showing a Waalbot prototype turning while climbing on a vertical acrylic surface. The prototype turns 90° (line overlayed) in six steps (bottom a–f).

The current Waalbot prototype was tested on a smooth clear acrylic climbing surface. It is capable of climbing any direction on a planes of various orientations. This includes climbing up, down, or across a vertical (90°) wall, all at the speed of 6 cm/s. The maximum angle which the prototype was able to climb was found to be 110° (20° past vertical).

The prototype Waalbot is able to make left and right hand turns without falling from the climbing surface (Fig. 11). Both small and large turning angles are routinely made. The prototype can be teleoperated to navigate around obstacles while climbing. Videos of the prototype performing various agility tasks can be viewed at [18].

Although analysis of plane to plane transitions (i.e. floor to wall) is beyond the scope of this paper, the robot design enables transitions of planes down to an acute 60°, and the prototype is able to transition from floor to vertical wall.

VI. Conclusion

A robot wall-climbing robot design was analyzed and implemented. A quasi-static model was created to determine the forces acting on the robot. A model for adhesive performance for a climbing robot was developed which demonstrates the margin of safety and steady state operating points. Design criteria were established to guide adhesive selection, foot size, and torque requirements. A semi-autonomous tetherless robot prototype was designed and fabricated which is able to climb on smooth surfaces of various orientations including a vertical surface. This robot can steer and turn with a small turning radius to travel along curved paths and around tight corners. IR communication is used to control the robot. The prototype was not able to climb on inverted surfaces, but was able to climb vertical (90°) surfaces and make floor to wall transitions.

One of the major disadvantages of this robot design is that there is very little redundancy in case of adhesion failure. At points during each gait cycle there are only two feet attached to the surface. Inverted walking has not been possible with the prototype due to the mass of the robot. As the adhesives used on the feet of the robot gather dust and other contaminants their performance degrades quickly. Therefore, these adhesives are not suitable for dirty outdoor environments, walking across indoor floors, or for long term tasks.

Future work includes studying other climbing surfaces and adhesives, as well as implementing the synthetic dry adhesives in place of the conventional adhesives when the technology is mature. Further miniaturization of the robots is required to improve performance due to increased area-to-mass ratio. Decreasing the robot mass will increase payload capacity, allowing for other sensors or tools and lower power consumption.

References

[1] W. Yan, L. Shuliang, X. Dianguo, Z. Yanzheng, S. Hao, and G. Xueshan, "Development and application of wall-climbing robots," in *IEEE Int. Conf. on Robotics and Automation*, 1999, pp. 1207–12.

[2] S. Hirose, A. Nagakubo, and R. Toyama, "Machine that can walk and climb on floors, walls and ceilings," in *Int. Conf. on Advanced Robotics*, vol. 1, 1991, pp. 753–758.

[3] S. Ryu, J. Park, S. Ryew, and H. Choi, "Self-contained wall-climbing robot with closed link mechanism," in *Int. Conf. on Intelligent Robots and Systems*, vol. 2, 2001, pp. 839 –844.

[4] L. Briones, P. Bustamante, and M. Serna, "Wall-climbing robot for inspection in nuclear power plants," in *IEEE Int. Conf. on Robotics and Automation*, 1994, pp. 1409–14.

[5] R. Pack, J. Christopher, J.L., and K. Kawamura, "A rubbertuator-based structure-climbing inspection robot," in *IEEE Int. Conf. on Robotics and Automation*, 1997, pp. 1869–74.

[6] B. Luk, A. Collie, V. Piefort, and G. Virk, "Robug iii: a tele-operated climbing and walking robot," in *UKACC Int. Conf. on Control*, vol. 1, 1996, pp. 347– 352.

[7] T. Yano, T. Suwa, M. Murakami, and T. Yamamoto, "Development of a semi self-contained wall climbing robot with scanning type suction cups," in *Int. Conf. on Intelligent Robots and Systems*, vol. 2, 1997, pp. 900–905.

[8] J. Grieco, M. Prieto, M. Armada, and P. Gonzalez de Santos, "A six-legged climbing robot for high payloads," in *IEEE Int. Conf. on Control Applications*, 1998, pp. 446–450.

[9] S. Kim, A. T. Asbeck, M. R. Cutkosky, and W. R. Provancher, "Spinybotii: Climbing hard walls with compliant microspines," in *Int. Conf. on Advanced Robotics*, 2005.

[10] T. Bretl, S. Rock, and J.-C. Latombe, "Motion planning for a three-limbed climbing robot in vertical natural terrain," in *IEEE Int. Conf. on Robotics and Automation*, 2003, pp. 2947–53.

[11] R. Altendorfer, N. Moore, H. Komsuoglu, M. Buehler, H. B. B. Jr., D. McMordie, U. Saranli, R. Full, and D. Koditschek, "Rhex: A biologically inspired hexapod runner." *Auton. Robots*, vol. 11, no. 3, pp. 207–213, 2001.

[12] R. Quinn, D. Kingsley, J. Offi, and R. Ritzmann, "Improved mobility through abstracted biological principles," in *IEEE Int. Conf. on Intelligent Robots and Systems*, 2002, pp. 2652–7.

[13] J. M. Morrey, B. Lambrecht, A. D. Horchler, R. E. Ritzmann, and R. D. Quinn, "Highly mobile and robust small quadruped robots," in *Intl. Conf. on Intelligent Robots and Systems*, vol. 1, 2003, pp. 82– 87.

[14] K. Daltorio, A. D. Horchler, S. Gorb2, R. Ritzmann, and R. Quinn, "A small wall-walking robot with compliant, adhesive feet," *Int. Conf. on Intelligent Robots and Systems*, pp. 4018–23, 2005.

[15] K. Autumn, Y. A. Liang, S. T. Hsieh, W. Zesch, W. P. Chan, T. W. Kenny, R. Fearing, and R. J. Full, "Adhesive force of a single gecko foot-hair," *Nature*, vol. 405, pp. 681–685, 2000.

[16] K. Autumn, M. Sitti, Y. A. Liang, A. M. Peattie, W. R. Hansen, S. Sponberg, T. W. Kenny, R. Fearing, J. N. Israelachvili, and R. J. Full, "Evidence for van der waals adhesion in gecko setae," *Proceedings of the National Academy of Sciences*, vol. 99, pp. 12 252–56, September 17 2002.

[17] C. Menon, M. Murphy, and M. Sitti, "Gecko inspired surface climbing robots," in *IEEE Int. Conf. on Robotics and Biomimetics (ROBIO)*, Shenyang, China, August 2004, pp. 431–436.

[18] [Online]. Available: http://nanolab.me.cmu.edu/projects/waalbots/tri-leg.html